Available online at www.sciencedirect.com
ScienceDirect
Probabilistic Engineering Mechanics 22 (2007) 27–38
PROBABILISTIC ENGINEERING MECHANICS
www.elsevier.com/locate/probengmech

Structural reliability analysis by univariate decomposition and numerical integration

D. Wei, S. Rahman*

Department of Mechanical and Industrial Engineering, The University of Iowa, Iowa City, IA 52242, United States

Received 22 July 2005; received in revised form 17 April 2006; accepted 1 May 2006
Available online 16 June 2006

Abstract

This paper presents a new and alternative univariate method for predicting component reliability of mechanical systems subject to random loads, material properties, and geometry. The method involves novel function decomposition at a most probable point that facilitates the univariate approximation of a general multivariate function in the rotated Gaussian space and one-dimensional integrations for calculating the failure probability. Based on linear and quadratic approximations of the univariate component function in the direction of the most probable point, two mathematical expressions of the failure probability have been derived. In both expressions, the proposed effort in evaluating the failure probability involves calculating conditional responses at a selected input determined by sample points and Gauss–Hermite integration points. Numerical results indicate that the proposed method provides accurate and computationally efficient estimates of the probability of failure.

Keywords: Reliability; Probability of failure; Decomposition methods; Most probable point; Univariate approximation; Numerical integration

1. Introduction

A fundamental problem in time-invariant component reliability analysis entails calculation of a multi-fold integral [1–3]

$$P_F \equiv P\left[g(\boldsymbol{X}) < 0\right] = \int_{g(\boldsymbol{x})<0} f_{\boldsymbol{X}}(\boldsymbol{x})\,\mathrm{d}\boldsymbol{x}, \tag{1}$$

where $\boldsymbol{X} = \{X_1, \ldots, X_N\}^{\mathrm{T}} \in \mathbb{R}^N$ is a real-valued, N-dimensional ($N \geq 2$) random vector defined on a probability space $(\Omega, \mathcal{F}, P)$ comprising the sample space Ω, the σ-field $\mathcal{F}$, and the probability measure P; $g(\boldsymbol{x})$ is the performance function, such that $g(\boldsymbol{x}) < 0$ represents the failure domain; P_F is the probability of failure; and $f_{\boldsymbol{X}}(\boldsymbol{x})$ is the joint probability density function of $\boldsymbol{X}$, which typically represents loads, material properties, and geometry. The most common approach to compute the failure probability in Eq. (1) involves the first- and second-order reliability methods (FORM/SORM) [1–8], which are respectively based on linear (FORM) and quadratic (SORM) approximations of the limit-state surface at a most probable point (MPP) in the standard Gaussian space. When the distance β_{HL} between the origin and the MPP, a point on the limit-state surface that is closest to the origin, approaches infinity, FORM/SORM strictly provides asymptotic solutions. For non-asymptotic (finite β_{HL}) applications involving a highly nonlinear performance function, its linear or quadratic approximation may not be adequate and therefore resultant FORM/SORM predictions must be interpreted with caution [9]. In the latter cases, an importance sampling method developed by Hohenbichler and Rackwitz [10] can make the FORM/SORM result arbitrarily exact, but it may become expensive if a large number of costly numerical analyses, such as large-scale finite element analysis embedded in the performance function, are involved. Furthermore, the existence of multiple MPPs may lead to large errors in standard FORM/SORM approximations [3,8]. In that case, multi-point FORM/SORM, along with the system reliability concept, is required to improve component reliability analysis [8].

Recently, the authors have developed new decomposition methods, which can solve highly nonlinear reliability problems more accurately or more efficiently than FORM/SORM and

* Corresponding author. Tel.: +1 319 335 5679; fax: +1 319 335 5669.
E-mail address: rahman@engineering.uiowa.edu (S. Rahman).
URL: http://www.engineering.uiowa.edu/~rahman (S. Rahman).

0266-8920/$ - see front matter © 2006 Elsevier Ltd. All rights reserved.
doi:10.1016/j.probengmech.2006.05.004

$$y(\boldsymbol{v}) = \underbrace{\underbrace{\underbrace{y_0 + \sum_{i=1}^{N} y_i(v_i)}_{=\hat{y}_1(\boldsymbol{v})} + \sum_{\substack{i_1,i_2=1 \\ i_1<i_2}}^{N} y_{i_1 i_2}(v_{i_1}, v_{i_2})}_{=\hat{y}_2(\boldsymbol{v})} + \cdots + \sum_{\substack{i_1,\ldots,i_S=1 \\ i_1<\cdots<i_S}}^{N} y_{i_1\cdots i_S}(v_{i_1}, \ldots, v_{i_s})}_{=\hat{y}_S(\boldsymbol{v})} + \cdots + y_{12\cdots N}(v_1, \ldots, v_N),$$

Box I.

simulation methods [11,12]. A major advantage of these decomposition methods, so far based on the mean point [11] or MPP [12] of a random input as reference points, over FORM/SORM is that higher-order approximations of performance functions can be achieved using function values alone. In particular, an MPP-based univariate method developed in the authors' previous work involves univariate approximation of the performance function at the MPP, n-point Lagrange interpolation in the rotated Gaussian space, and subsequent Monte Carlo simulation [12]. The present work is motivated by an argument that the MPP-based univariate approximation, if appropriately cast in the rotated Gaussian space, permits an efficient evaluation of the component failure probability by multiple one-dimensional integrations.

This paper presents a new and alternative MPP-based univariate method for predicting the component reliability of mechanical systems subject to random loads, material properties, and geometry. Section 2 gives a brief exposition of a novel function decomposition at the MPP that facilitates a lower-dimensional approximation of a general multivariate function. Section 3 describes the proposed univariate method, which involves univariate approximation of the performance function at the MPP and univariate numerical integrations. Section 4 explains the computational effort and flowchart of the proposed method. Five numerical examples involving elementary mathematical functions and structural/solid-mechanics problems illustrate the method developed in Section 5. Comparisons have been made with alternative approximate and simulation methods to evaluate the accuracy and computational efficiency of the new method.

2. Multivariate function decomposition at MPP

Consider a continuous, differentiable, real-valued performance function $g(\boldsymbol{x})$ that depends on $\boldsymbol{x} = \{x_1, \ldots, x_N\}^{\mathrm{T}} \in \mathbb{R}^N$. If $\boldsymbol{u} = \{u_1, \ldots, u_N\}^{\mathrm{T}} \in \mathbb{R}^N$ is the standard Gaussian space, let $\boldsymbol{u}^* = \{u_1^*, \ldots, u_N^*\}^{\mathrm{T}}$ denote the MPP or beta point, which is the closest point on the limit-state surface to the origin. The MPP has a distance β_{HL}, which is commonly referred to as the Hasofer–Lind reliability index [1–3], determined by a standard nonlinear constrained optimization. Construct an orthogonal matrix $\boldsymbol{R} \in \mathbb{R}^{N\times N}$ whose Nth column is $\boldsymbol{\alpha}^* \equiv \boldsymbol{u}^*/\beta_{\mathrm{HL}}$, i.e., $\boldsymbol{R} = [\boldsymbol{R}_1 \mid \boldsymbol{\alpha}^*]$, where $\boldsymbol{R}_1 \in \mathbb{R}^{N\times N-1}$ satisfies $\boldsymbol{\alpha}^{*\mathrm{T}}\boldsymbol{R}_1 = \boldsymbol{0} \in \mathbb{R}^{1\times N-1}$. The matrix $\boldsymbol{R}$ can be obtained, for example, by Gram–Schmidt orthogonalization. For an orthogonal transformation $\boldsymbol{u} = \boldsymbol{R}\boldsymbol{v}$, let $\boldsymbol{v} = \{v_1, \ldots, v_N\}^{\mathrm{T}} \in \mathbb{R}^N$ represent the rotated Gaussian space with the associated MPP

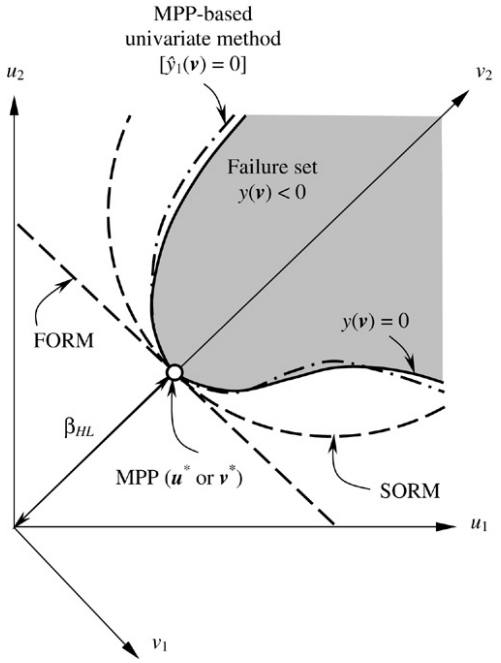

Fig. 1. Performance function approximations by various methods.

$\boldsymbol{v}^* = \{v_1^*, \ldots, v_{N-1}^*, v_N^*\}^{\mathrm{T}} = \{0, \ldots, 0, \beta_{\mathrm{HL}}\}^{\mathrm{T}}$. The transformed limit states $h(\boldsymbol{u}) = 0$ and $y(\boldsymbol{v}) = 0$ are therefore the maps of the original limit state $g(\boldsymbol{x}) = 0$ in the standard Gaussian space ($\boldsymbol{u}$ space) and the rotated Gaussian space ($\boldsymbol{v}$ space), respectively. Fig. 1 depicts FORM and SORM approximations of a limit-state surface at the MPP for $N = 2$.

Consider a decomposition of a general multivariate function $y(\boldsymbol{v})$, which can be viewed as a finite sum [11–13] (see Box I), where y_0 is a constant, $y_i(v_i)$ is a univariate component function representing an individual contribution to $y(\boldsymbol{v})$ by input variable v_i acting alone, $y_{i_1 i_2}(v_{i_1}, v_{i_2})$ is a bivariate component function describing the cooperative influence of two input variables v_{i_1} and v_{i_2}, $y_{i_1\cdots i_S}(v_{i_1}, \ldots, v_{i_S})$ is an S-variate component function quantifying the cooperative effects of S input variables $v_{i_1}, \ldots, v_{i_S}$, and so on. If

$$\hat{y}_S(\boldsymbol{v}) = y_0 + \sum_{i=1}^{N} y_i(v_i) + \sum_{\substack{i_1,i_2=1 \\ i_1<i_2}}^{N} y_{i_1 i_2}(v_{i_1}, v_{i_2}) + \cdots + \sum_{\substack{i_1,\ldots,i_S=1 \\ i_1<\cdots<i_S}}^{N} y_{i_1\cdots i_S}(v_{i_1}, \ldots, v_{i_s}) \tag{2}$$

represents a general S-variate approximation of $y(\boldsymbol{v})$, the univariate ($S = 1$) and bivariate ($S = 2$) approximations

$\hat{y}_1(\boldsymbol{v})$ and $\hat{y}_2(\boldsymbol{v})$ respectively provide two- and three-term approximants of the finite decomposition in the equation given in Box I. Similarly, trivariate, quadrivariate, and other higher-variate approximations can be derived by appropriately selecting the value of S. In the limit when $S = N$, $\hat{y}_S(\boldsymbol{v})$ converges to the exact function $y(\boldsymbol{v})$. In other words, the decomposition in Eq. (2) generates a convergent sequence of approximations of $y(\boldsymbol{v})$. Readers interested in the fundamental development of the decomposition are referred to Xu and Rahman [13].

3. New univariate method

3.1. Univariate decomposition of performance function

Consider a univariate approximation of $y(\boldsymbol{v})$, denoted by

$$\begin{aligned}\hat{y}_1(\boldsymbol{v}) &\equiv \hat{y}_1(v_1,\ldots,v_N)\\ &= \sum_{i=1}^{N} y(v_1^*,\ldots,v_{i-1}^*,v_i,v_{i+1}^*,\ldots,v_N^*)\\ &\quad -(N-1)y(\boldsymbol{v}^*),\end{aligned} \tag{3}$$

where each term in the summation is a function of only one variable and can subsequently be expanded in a Taylor series at the MPP, $\boldsymbol{v}^* = \left\{v_1^*,\ldots,v_{N-1}^*,v_N^*\right\}^{\mathrm{T}} = \{0,\ldots,0,\beta_{\mathrm{HL}}\}^{\mathrm{T}}$, yielding

$$\hat{y}_1(\boldsymbol{v}) = y(\boldsymbol{v}^*) + \sum_{j=1}^{\infty}\frac{1}{j!}\sum_{i=1}^{N}\frac{\partial^j y}{\partial v_i^j}\left(\boldsymbol{v}^*\right)(v_i - v_i^*)^j. \tag{4}$$

In contrast, the Taylor series expansion of $y(\boldsymbol{v})$ at $\boldsymbol{v}^* = \left\{v_1^*,\ldots,v_N^*\right\}^{\mathrm{T}}$ can be expressed by

$$y(\boldsymbol{v}) = y\left(\boldsymbol{v}^*\right) + \sum_{j=1}^{\infty}\frac{1}{j!}\sum_{i=1}^{N}\frac{\partial^j y}{\partial v_i^j}\left(\boldsymbol{v}^*\right)\left(v_i - v_i^*\right)^j + \mathcal{R}_2 \tag{5}$$

where the remainder $\mathcal{R}_2$ denotes all terms with dimensions two and higher. A comparison of Eqs. (4) and (5) indicates that the univariate approximation of $\hat{y}_1(\boldsymbol{v})$ leads to a residual error $y(\boldsymbol{v}) - \hat{y}_1(\boldsymbol{v}) = \mathcal{R}_2$, which includes contributions from terms of dimension two and higher. For sufficiently smooth $y(\boldsymbol{v})$ with a convergent Taylor series, the coefficients associated with higher-dimensional terms are usually much smaller than those with one-dimensional terms. As such, higher-dimensional terms contribute less to the function, and therefore can be neglected. Nevertheless, Eq. (3) includes all higher-order *univariate* terms, compared with FORM and SORM, which only retain *linear and quadratic univariate* terms, respectively. If the univariate decomposition is not sufficient, bivariate or higher-variate decompositions may be required [11]. Because of the higher cost, these were not included in this study.

In addition to the MPP as the chosen reference point, the accuracy of the univariate approximation in Eq. (3) may depend on the orientation of the first $N-1$ axes. In this work, the orientation is defined by the matrix $\boldsymbol{R}$. However, an improved approximation may be possible by selecting an orientation that is optimal in some sense. This issue was not considered in the present work.

3.2. Univariate integration for failure probability analysis

The proposed univariate approximation of the performance function can be rewritten as

$$\hat{y}_1(\boldsymbol{v}) = y_N(v_N) + \sum_{i=1}^{N-1} y_i(v_i) - (N-1)y(\boldsymbol{v}^*), \tag{6}$$

where $y_i(v_i) \equiv y(v_1^*,\ldots,v_{i-1}^*,v_i,v_{i+1}^*,\ldots,v_N^*); i = 1,N$. Due to rotational transformation of the coordinates (see Fig. 1), the univariate component function $y_N(v_N)$ in Eq. (6) is expected to be a linear or a weakly nonlinear function of v_N. In fact, $y_N(v_N)$ is linear with respect to v_N in the classical FORM/SORM approximation of a performance function in the $\boldsymbol{v}$ space. Nevertheless, if $y_N(v_N)$ is invertible, the univariate approximation $\hat{y}_1(\boldsymbol{v})$ can be further expressed in a form amenable to an efficient reliability analysis by one-dimensional numerical integration. In this work, both linear and quadratic approximations of $y_N(v_N)$ and the resultant equations for failure probability are derived, as follows.

3.2.1. Linear approximation of $y_N(v_N)$

Consider a linear approximation: $y_N(v_N) = b_0 + b_1 v_N$, where coefficients $b_0 \in \mathbb{R}$ and $b_1 \in \mathbb{R}$ (non-zero) are obtained by least-squares approximations from exact or numerically simulated responses $\left\{y_N(v_N^{(1)}),\ldots,y_N(v_N^{(n)})\right\}$ at n sample points along the v_N coordinate. The least-squares approximation was chosen over interpolation, because the former minimizes the error when $n > 2$. Applying the linear approximation, the component failure probability can be expressed by

$$\begin{aligned}P_F &\equiv P\left[y(\boldsymbol{V}) < 0\right] \cong P\left[\hat{y}_1(\boldsymbol{V}) < 0\right]\\ &\cong P\left[b_0 + b_1 V_N + \sum_{i=1}^{N-1} y_i(V_i) - (N-1)y(\boldsymbol{v}^*) < 0\right],\end{aligned} \tag{7}$$

which, on inversion, yields

$$P_F \cong \begin{cases} P\left[V_N < \dfrac{(N-1)y(\boldsymbol{v}^*) - b_0}{b_1} - \dfrac{1}{b_1}\displaystyle\sum_{i=1}^{N-1} y_i(V_i)\right], \\ \quad \text{if } b_1 > 0 \\ P\left[V_N \geq \dfrac{(N-1)y(\boldsymbol{v}^*) - b_0}{b_1} - \dfrac{1}{b_1}\displaystyle\sum_{i=1}^{N-1} y_i(V_i)\right], \\ \quad \text{if } b_1 < 0. \end{cases} \tag{8}$$

Since V_N follows standard Gaussian distribution, the failure probability can also be expressed by

$$P_F \cong \mathbb{E}\left[\Phi\left(\frac{(N-1)y(\boldsymbol{v}^*) - b_0}{|b_1|} - \frac{1}{|b_1|}\sum_{i=1}^{N-1} y_i(V_i)\right)\right], \tag{9}$$

where $\mathbb{E}$ is the expectation operator and $\Phi(u) = \left(1/\sqrt{2\pi}\right)\int_{-\infty}^{u}\exp\left(-\xi^2/2\right)\mathrm{d}\xi$ is the cumulative distribution function of a standard Gaussian random variable. Note that Eq. (9) provides higher-order estimates of failure probability if univariate component functions $y_i(v_i)$, $i = 1, N-1$, are approximated

by terms higher than second order. If $y_i(v_i)$, $i = 1, N-1$, retain only linear and quadratic terms fitted with appropriately selected sample points, Eq. (9) can be further simplified to degenerate to the well-known FORM and SORM (point-fitted) approximations.

3.2.2. Quadratic approximation of $y_N(v_N)$

The linear approximation described in the preceding can be improved by a quadratic approximation: $y_N(v_N) = b_0 + b_1 v_N + b_2 v_N^2$, where coefficients $b_0 \in \mathbb{R}$, $b_1 \in \mathbb{R}$, and $b_2 \in \mathbb{R}$ (non-zero) are also obtained by least-squares approximations from exact or numerically simulated responses at n sample points along the v_N coordinate. Again, the least-squares approximation was selected due to error minimization when $n > 3$. Similarly, the quadratic approximation of $y_N(v_N)$ employed in Eq. (6) leads to

$$P_F \equiv P\left[y(\boldsymbol{V}) < 0\right] \cong P\left[\hat{y}_1(\boldsymbol{V}) < 0\right] \cong P\left[b_0 + b_1 V_N + b_2 V_N^2 + \sum_{i=1}^{N-1} y_i(V_i) - (N-1)y(\boldsymbol{v}^*) < 0\right]. \tag{10}$$

By defining $B(\tilde{\boldsymbol{V}}) \equiv b_0 + \sum_{i=1}^{N-1} y_i(V_i) - (N-1)y(\boldsymbol{v}^*)$, where $\tilde{\boldsymbol{V}} = \{V_1, \ldots, V_{N-1}\}^{\mathrm{T}}$ is an $N-1$-dimensional standard Gaussian vector, the following solutions are derived on the basis of two cases:

(a) *Case I — Trivial Solution* ($b_1{}^2 - 4b_2 B < 0$; *no real roots*):

$$P_F \cong \begin{cases} 0, & \text{if } b_2 > 0 \\ 1, & \text{if } b_2 < 0. \end{cases} \tag{11}$$

(b) *Case II — Non-Trivial Solution* ($b_1{}^2 - 4b_2 B \geq 0$; *two real roots*):

$$P_F \cong \begin{cases} P\left[\dfrac{-b_1 - \sqrt{b_1{}^2 - 4b_2 B(\tilde{\boldsymbol{V}})}}{2b_2} < V_N < \dfrac{-b_1 + \sqrt{b_1{}^2 - 4b_2 B(\tilde{\boldsymbol{V}})}}{2b_2}\right], & \text{if } b_2 > 0 \\ 1 - P\left[\dfrac{-b_1 + \sqrt{b_1{}^2 - 4b_2 B(\tilde{\boldsymbol{V}})}}{2b_2} < V_N < \dfrac{-b_1 - \sqrt{b_1{}^2 - 4b_2 B(\tilde{\boldsymbol{V}})}}{2b_2}\right], & \text{if } b_2 < 0, \end{cases} \tag{12}$$

yielding

$$P_F \cong \frac{1 - b_2/|b_2|}{2} + \mathbb{E}\left[\Phi\left(\frac{-b_1 + \sqrt{b_1{}^2 - 4b_2 B(\tilde{\boldsymbol{V}})}}{2b_2}\right)\right] - \mathbb{E}\left[\Phi\left(\frac{-b_1 - \sqrt{b_1{}^2 - 4b_2 B(\tilde{\boldsymbol{V}})}}{2b_2}\right)\right]. \tag{13}$$

Both Eqs. (9) and (13) can be employed for non-trivial solutions of failure probability. Improvement in the accuracy of results, if any, depends on how strongly $y_N(v_N)$ depends on v_N. Furthermore, it is possible to develop a generalized version of Eq. (13) when $y_N(v_N)$ is highly nonlinear (e.g. polynomial of an arbitrary order), but invertible. However, due to the rotational transformation from the $\boldsymbol{x}$ space to the $\boldsymbol{v}$ space, it is expected that the linear approximation of $y_N(v_N)$ (Eq. (9)) should result in a very accurate solution. Hence, the present study is limited to only linear and quadratic approximations of $y_N(v_N)$. It is worth noting that, unlike Eq. (9), Eq. (13) cannot be reduced to FORM/SORM equations, as $y_N(v_N)$ includes a second-order term.

3.2.3. Univariate integration

The failure probability expressions in Eqs. (9) and (13) involve the calculation of the expected values of several multivariate functions of an $N-1$-dimensional standard Gaussian vector $\tilde{\boldsymbol{V}} = \{V_1, \ldots, V_{N-1}\}^{\mathrm{T}}$. A generic expression for such a calculation requires the determination of $\mathbb{E}[\Phi(f(\tilde{\boldsymbol{V}}))]$, where $f : \mathbb{R}^{N-1} \mapsto \mathbb{R}$ is a general mapping of $\tilde{\boldsymbol{V}}$ and depends on how univariate component functions $y_i(v_i), i = 1, N-1$, are approximated. Unfortunately, the exact probability density function of $f(\tilde{\boldsymbol{V}})$ is, in general, not available in closed form. For this reason, it is difficult to calculate $\mathbb{E}[\Phi(f(\tilde{\boldsymbol{V}}))]$ analytically. Numerical integration is not efficient, as $\Phi(f(\tilde{\boldsymbol{v}}))$ is a multivariate function and becomes impractical when the dimension exceeds three or four.

In reference to Eq. (3), again consider a univariate approximation of

$$\ln\left[\Phi\left(f(\tilde{\boldsymbol{v}})\right)\right] \cong \sum_{i=1}^{N-1} \ln\left[\Phi\left(f_i(v_i)\right)\right] - (N-2)\ln\left[\Phi\left(f(\tilde{\boldsymbol{v}}^*)\right)\right], \tag{14}$$

where $f_i(v_i) \equiv f(v_1^*, \ldots, v_{i-1}^*, v_i, v_{i+1}^*, \ldots, v_{N-1}^*)$; $i = 1, N-1$ are univariate component functions; and $f(\tilde{\boldsymbol{v}}^*) \equiv f(v_1^*, \ldots, v_{N-1}^*)$. Hence

$$\Phi\left(f(\tilde{\boldsymbol{v}})\right) = \exp\left\{\ln\left[\Phi\left(f(\tilde{\boldsymbol{v}})\right)\right]\right\} \cong \exp\left\{\sum_{i=1}^{N-1} \ln\left[\Phi\left(f_i(v_i)\right)\right] - (N-2)\ln\left[\Phi\left(f(\tilde{\boldsymbol{v}}^*)\right)\right]\right\} = \frac{\prod_{i=1}^{N-1} \Phi\left(f_i(v_i)\right)}{\Phi\left(f(\tilde{\boldsymbol{v}}^*)\right)^{N-2}}, \tag{15}$$

yielding

$$\mathbb{E}[\Phi(f(\tilde{\boldsymbol{V}}))] \cong \frac{\prod_{i=1}^{N-1} \mathbb{E}\left[\Phi\left(f_i(V_i)\right)\right]}{\Phi\left(f(\tilde{\boldsymbol{v}}^*)\right)^{N-2}} = \frac{\prod_{i=1}^{N-1} \int_{-\infty}^{+\infty} \Phi\left(f_i(v_i)\right)\phi(v_i)\,\mathrm{d}v_i}{\Phi\left(f(\tilde{\boldsymbol{v}}^*)\right)^{N-2}}, \tag{16}$$

which involves a product of $N-1$ *univariate* integrals with $\phi(\cdot)$ denoting the standard Gaussian probability density function. Using Eq. (16), the nontrivial expressions of failure probability in Eqs. (9) and (13) are

$$P_F \cong \frac{\prod_{i=1}^{N-1} \int_{-\infty}^{+\infty} \Phi\left(\frac{(N-1)y(\boldsymbol{v}^*)-b_0-y_i(v_i)}{|b_1|}\right)\phi(v_i)\,\mathrm{d}v_i}{\left[\Phi\left(\frac{(N-1)y(\boldsymbol{v}^*)-b_0-\sum_{i=1}^{N-1} y_i(\boldsymbol{v}_i^*)}{|b_1|}\right)\right]^{N-2}} \tag{17}$$

and

$$P_F \cong \frac{1-b_2/|b_2|}{2} + \left\{\frac{\prod_{i=1}^{N-1} \int_{-\infty}^{+\infty} \Phi\left(\frac{-b_1+\sqrt{b_1{}^2-4b_2B_i(v_i)}}{2b_2}\right)\phi(v_i)\,\mathrm{d}v_i}{\left[\Phi\left(\frac{-b_1+\sqrt{b_1{}^2-4b_2B(\tilde{\boldsymbol{v}}^*)}}{2b_2}\right)\right]^{N-2}} - \frac{\prod_{i=1}^{N-1} \int_{-\infty}^{+\infty} \Phi\left(\frac{-b_1-\sqrt{b_1{}^2-4b_2B_i(v_i)}}{2b_2}\right)\phi(v_i)\,\mathrm{d}v_i}{\left[\Phi\left(\frac{-b_1+\sqrt{b_1{}^2-4b_2B(\tilde{\boldsymbol{v}}^*)}}{2b_2}\right)\right]^{N-2}}\right\} \tag{18}$$

respectively, where $B_i(v_i) \equiv B(v_1^*, \ldots, v_{i-1}^*, v_i, v_{i+1}^*, \ldots, v_{N-1}^*)$. The univariate integration involved in Eqs. (17) or (18) can be evaluated easily by standard one-dimensional Gauss–Hermite numerical quadrature [14]. The decomposition method involving univariate approximation (Eq. (3)) and univariate integration (Eqs. (17) or (18)) is defined as the *MPP-based univariate method with numerical integration* in this paper.

4. Computational effort and flow

Consider $y_i(v_i) \equiv y(v_1^*, \ldots, v_{i-1}^*, v_i, v_{i+1}^*, \ldots, v_N^*)$, $i = 1, N-1$, for which n function values $y_i(v_i^{(j)}) \equiv y(v_1^*, \ldots, v_{i-1}^*, v_i^{(j)}, v_{i+1}^*, \ldots, v_N^*)$, $j = 1, \ldots, n$, are required to be evaluated at integration points $v_i = v_i^{(j)}$ to perform an n-order Gauss–Hermite quadrature for the ith integration in Eqs. (17) or (18). The same procedure is repeated for $N-1$ univariate component functions, i.e. for all $y_i(v_i)$, $i = 1, \ldots, N-1$. Therefore, the total cost of the proposed univariate method, including the n function values of $y_N(v_N)$ required for its linear or quadratic approximation, entails a *maximum* of nN function evaluations.[1] Note that the above cost is in addition to any function evaluations required for locating the MPP.

Fig. 2 shows the computational flowchart of the MPP-based univariate method with numerical integration. The implementation of the method requires the calculation of $y_N(v_N)$ at a user-selected input to obtain coefficients b_0, b_1, and/or b_2 and the calculation of $y_i(v_i)$, $i = 1, \ldots, N-1$, at Gauss–Hermite integration points to perform the numerical integration. Both calculations entail the evaluation of univariate component functions, which are conditional responses. Hence, the proposed effort in determining the failure probability can be viewed as numerically calculating conditional responses at a selected input. Compared with the previously developed univariate method [12], no Monte Carlo simulation is required in the present method. The accuracy and efficiency of the new method depend on both the univariate approximation and numerical integration. They will be evaluated using several numerical examples in a forthcoming section.

In performing n-order Gauss–Hermite quadratures in Eqs. (17) or (18), two options for evaluating $y_i(v_i)$ are proposed. Option 1 involves calculating $y_i(v_i^{(j)})$ at integration points $(v_1^*, \ldots, v_{i-1}^*, v_i^{(j)}, v_{i+1}^*, \ldots, v_N^*)$, $j = 1, n$, from direct numerical analysis (e.g. finite-element analysis). When the computation of $y_i(v_i)$ is expensive, the first option is inefficient if n is required to be large for accurate numerical integration. The second option involves developing first a univariate response-surface approximation of $y_i(v_i)$ from selected sample points in the v_i-coordinate, followed by numerical integration of the response-surface approximation. Option 2 is computationally efficient, because no additional numerical analysis (e.g. finite-element analysis) is required if the order of integration is larger than the number of sample points. However, an additional layer of response-surface approximation is involved in the second option. Both options were explored in numerical examples, as follows.

5. Numerical examples

Five numerical examples involving explicit performance functions from mathematical or solid-mechanics problems (Examples 1 and 2) and implicit functions from structural or solid-mechanics problems (Examples 3, 4, and 5) are presented to illustrate the MPP-based univariate method with numerical integration. Whenever possible, comparisons have been made with the previously developed MPP-based univariate method with simulation [12], FORM/SORM, and direct Monte Carlo simulation to evaluate the accuracy and efficiency of the new method.

To obtain the linear or quadratic approximation of $y_N(v_N)$, n (= 5, 7 or 9) sample points $v_N^* - (n-1)/2, v_N^* - (n-3)/2, \ldots, v_N^*, \ldots, v_N^* + (n-3)/2, v_N^* + (n-1)/2$ were deployed along the v_N-coordinate. The same value of n was employed as the order of Gauss–Hermite quadratures in Eqs. (17) or (18) of the proposed univariate method with numerical integration. Furthermore, option 1 was used in Examples 3 and 4 and option 2 was invoked in Examples 1, 2 and 5. When using option 2, an nth-order polynomial equation was employed for generating the response-surface approximation of various component functions $y_i(v_i)$, $i = 1, N-1$. A 10-order Gauss–Hermite integration was invoked in option 2. For a consistent comparison, the same value of n was also employed as the number of sample points in the previously developed univariate method with simulation [12]. Hence, the

[1] The orders of numerical integration and the number of function values of $y_N(v_N)$ need not be the same. In addition, different orders of integration can be employed if desired.

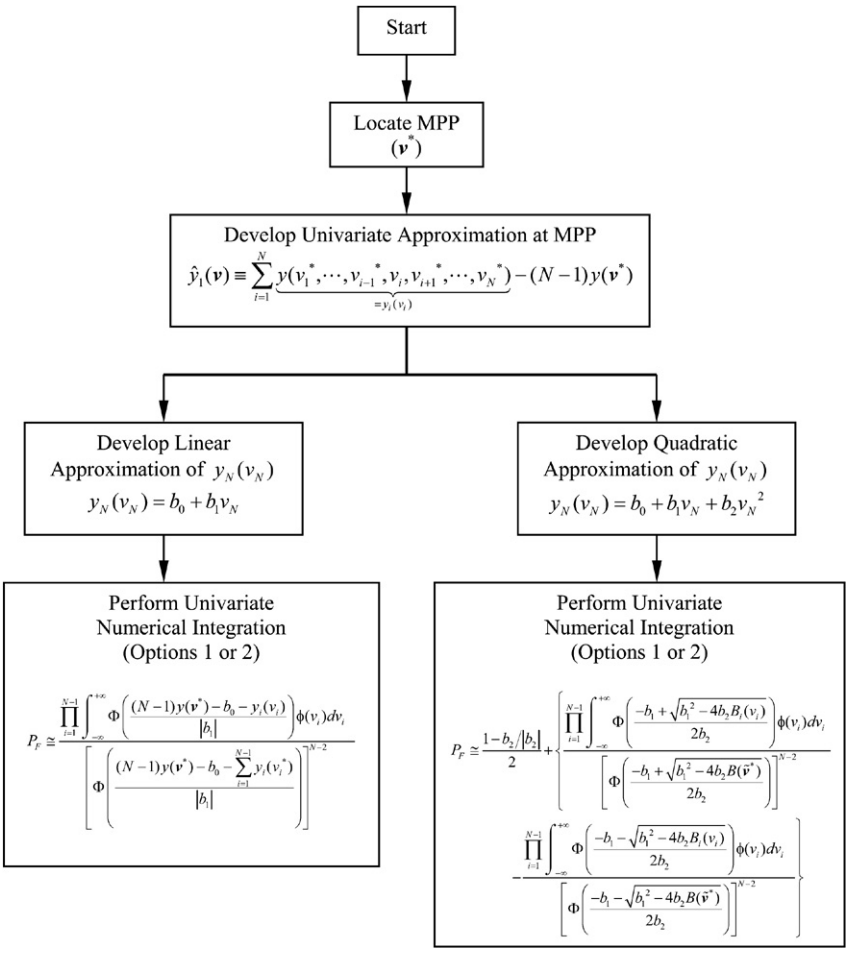

Fig. 2. Flowchart of the MPP-based univariate method with numerical integration.

total number of function evaluations required by both versions of the univariate method, in addition to those required for locating the MPP, is $(n-1)N$. When comparing computational efforts by various methods, the number of *original* performance function evaluations is chosen as the primary metric in this paper.

5.1. Example 1 — Elementary mathematical functions

Consider cubic and quartic performance functions, expressed respectively by [12]

$$g(X_1, X_2) = 2.2257 - \frac{0.025\sqrt{2}}{27}(X_1 + X_2 - 20)^3 + \frac{33}{140}(X_1 - X_2) \tag{19}$$

$$g(X_1, X_2) = \frac{5}{2} + \frac{1}{216}(X_1 + X_2 - 20)^4 - \frac{33}{140}(X_1 - X_2), \tag{20}$$

where X_i, $i = 1, 2$, are independent, Gaussian random variables, each with mean $\mu = 10$ and standard deviation $\sigma = 3$. From an MPP search, $\boldsymbol{v}^* = \{0, 2.2257\}^{\mathrm{T}}$ and $\beta_{\mathrm{HL}} = \|\boldsymbol{v}^*\| = 2.2257$ for the cubic function and $\boldsymbol{v}^* = \{0, 2.5\}^{\mathrm{T}}$ and $\beta_{\mathrm{HL}} = \|\boldsymbol{v}^*\| = 2.5$ for the quartic function. For both variants of the univariate method, a value of $n = 5$ was selected, resulting in nine function evaluations. Since both performance functions in the rotated Gaussian space are linear in v_2, the proposed method involving Eq. (17) was employed to calculate the failure probability.

Tables 1 and 2 show the results of the failure probability calculated by FORM, SORM [4–6], the MPP-based univariate method with simulation [12], the proposed MPP-based univariate method with numerical integration, and direct Monte Carlo simulation using 10^6 samples. The univariate method with simulation, which yields exact limit-state equations in this particular example, predicts the same probability of failure by the direct Monte Carlo simulation. The univariate method with numerical integration also yields exact limit-state equations and predicts very accurate estimates of failure probability when compared with simulation results. A slight difference in the failure probability estimates by two versions of the univariate method is due to the approximations involved in Eqs. (7) and (14) of the proposed method. Nevertheless, other commonly used reliability methods, such as FORM and SORM, underpredict the failure probability by 31% and overpredict the failure probability by 117% compared with the direct Monte Carlo results. The SORM results are the same as the FORM results, indicating that there is no improvement over FORM for

Table 1
Failure probability for cubic performance function

Method	Failure probability	Number of function evaluations[a]
MPP-based univariate method with numerical integration	0.01895	29[b]
MPP-based univariate method with simulation [12]	0.01907	29[b]
FORM	0.01302	21
SORM [4–6]	0.01302	204
Direct Monte Carlo simulation	0.01907	1000,000

[a] Total number of times that the original performance function is calculated.
[b] $21 + (n-1) \times N = 21 + (5-1) \times 2 = 29$.

Table 2
Failure probability for quartic performance function

Method	Failure probability	Number of function evaluations[a]
MPP-based univariate method with numerical integration	0.003030	29[b]
MPP-based univariate method with simulation [12]	0.002886	29[b]
FORM	0.006209	21
SORM [4–6]	0.006208	212
Direct Monte Carlo simulation	0.002886	1000,000

[a] Total number of times that the original performance function is calculated.
[b] $21 + (n-1) \times N = 21 + (5-1) \times 2 = 29$.

problems involving an inflection point (cubic function) or high nonlinearity (quartic function).

5.2. Example 2 — Burst margin of a rotating disk

Consider an annular disk of inner radius R_i, outer radius R_o, and constant thickness $t \ll R_o$ (plane stress), as shown in Fig. 3. The disk is subject to an angular velocity, ω, about an axis perpendicular to its plane at the centre. The maximum allowable angular velocity, ω_a, when tangential stresses through the thickness reach the material's ultimate strength, S_u, factored by a material utilization factor α_m, is [15]

$$\omega_a = \left[\frac{3\alpha_m S_u\,(R_o - R_i)}{\rho\left(R_o^3 - R_i^3\right)}\right]^{1/2}, \tag{21}$$

where ρ is the mass density of the material. According to an SAE G-11 standard, the satisfactory performance of the disk is defined when the burst margin M_b, defined as

$$M_b \equiv \frac{\omega_a}{\omega} = \left[\frac{3\alpha_m S_u\,(R_o - R_i)}{\rho\omega^2\left(R_o^3 - R_i^3\right)}\right]^{1/2}, \tag{22}$$

exceeds 0.374 73 [16]. If random variables $X_1 = \alpha_m$, $X_2 = S_u$, $X_3 = \omega$, $X_4 = \rho$, $X_5 = R_o$, and $X_6 = R_i$ have their statistical properties defined in Table 3, the performance function becomes

$$g(\boldsymbol{X}) = M_b(X_1, X_2, X_3, X_4, X_5, X_6) - 0.374\,73. \tag{23}$$

Table 4 presents the predicted failure probability of the disk and the associated computational effort using new and existing MPP-based univariate methods, FORM, Hohenbichler's SORM [5], and direct Monte Carlo simulation (10^6 samples). For univariate methods, a value of $n = 7$ was selected. For the univariate method with numerical integration, the failure probabilities based on linear (Eq. (17)) and quadratic (Eq. (18)) approximations are almost identical, which verifies the adequacy of the linear approximation of $y_N(v_N)$ in this example. The results also indicate that the univariate methods using either simulation or numerical integration produce the most accurate solution. FORM and SORM slightly underpredict the failure probability. Both univariate methods surpass the efficiency of SORM in solving this particular reliability problem.

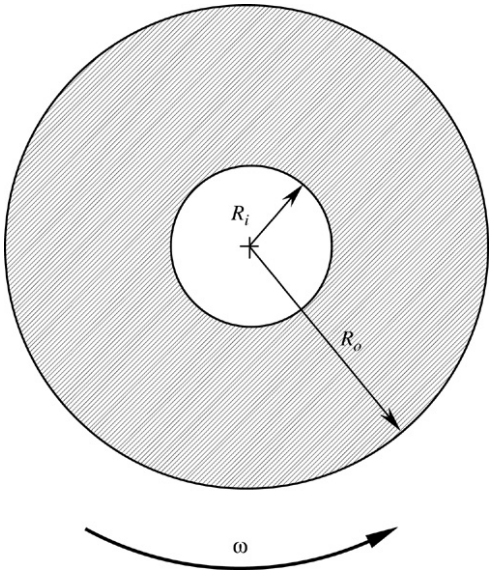

Fig. 3. Rotating annular disk subject to angular velocity.

5.3. Example 3 — Ten-bar truss structure

A ten-bar, linear-elastic, truss structure, shown in Fig. 4, was studied in this example to examine the accuracy and efficiency of the proposed reliability method. The Young's

Table 3
Statistical properties of random input for rotating disk

Random variable	Mean	Standard deviation	Probability distribution
α_m	0.9377	0.0459	Weibull[a]
S_u, ksi	220	5	Gaussian
ω, rpm	24	0.5	Gaussian
ρ, lb $-$ s^2/in.^{4}	$0.29/g$[b]	$0.0058/g$[b]	Uniform[c]
R_o, in.	24	0.5	Gaussian
R_i, in.	8	0.3	Gaussian

[a] Scale parameter = 25.508; shape parameter = 0.958.
[b] $g = 385.82$ in./s^2.
[c] Uniformly distributed over (0.28, 0.3).

Table 4
Failure probability of rotating disk

Method	Failure probability	Number of function evaluations[a]
MPP-based univariate method with numerical integration		
Linear (Eq. (17))	0.00099	167[b]
Quadratic (Eq. (18))	0.00099	167[b]
MPP-based univariate method with simulation [12]	0.00101	167[b]
FORM	0.00089	131
SORM (Hohenbichler) [5]	0.00097	378
Direct Monte Carlo simulation	0.00104	1000,000

[a] Total number of times that the original performance function is calculated.
[b] $131 + (n-1) \times N = 131 + (7-1) \times 6 = 167$.

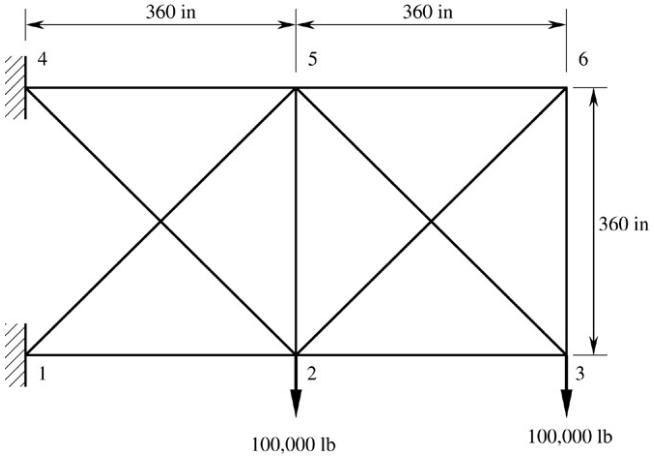

Fig. 4. A ten-bar truss structure.

modulus of the material is 10^7 psi. Two concentrated forces of 10^5 lb are applied at nodes 2 and 3, as shown in Fig. 4. The cross-sectional area X_i, $i = 1, \ldots, 10$ for each bar follows a truncated normal distribution clipped at $x_i = 0$ and has mean $\mu = 2.5$ in.^{2} and standard deviation $\sigma = 0.5$ in.^{2}. According to the loading condition, the maximum displacement $[v_3(X_1, \ldots, X_{10})]$ occurs at node 3, where the permissible displacement is limited to 18 in., leading to $g(\boldsymbol{X}) = 18 - v_3(X_1, \ldots, X_{10})$.

From an MPP search involving finite-difference gradients, $\beta_{\mathrm{HL}} = \|\boldsymbol{v}^*\| = 1.3642$. Table 5 shows the failure probability of the truss, calculated using the proposed MPP-based univariate method with numerical integration, MPP-based univariate method with simulation [12], FORM, three variants of SORM due to Breitung [4], Hohenbichler [5] and Cai and Elishakoff [6], and direct Monte Carlo simulation (10^6 samples). For univariate methods, a value of $n = 7$ was selected. From Table 5, both versions of the univariate method predict the failure probability more accurately than FORM and all three variants of SORM. This is because univariate methods are able to approximate the performance function more accurately than FORM/SORM. The univariate method with numerical integration involving the quadratic approximation of $y_N(v_N)$ yields a slightly more accurate result than that based on its linear approximation. A comparison of the number of function evaluations, also listed in Table 5, indicates that the computational effort by the MPP-based univariate methods is slightly larger than FORM, but much less than SORM.

5.4. Example 4 — Mixed-mode fracture-mechanics analysis

The fourth example involves an isotropic, homogeneous, edge-cracked plate, presented to illustrate mixed-mode probabilistic fracture-mechanics analysis using the proposed univariate method. As shown in Fig. 5(a), a plate of length $L = 16$ units and width $W = 7$ units is fixed at the bottom and subjected to a far-field and a shear stress τ^∞ applied at the top. The elastic modulus and Poisson's ratio are 1 unit and 0.25, respectively. A plane strain condition was assumed. The statistical property of the random input $\boldsymbol{X} = \{a/W, \tau^\infty, K_{Ic}\}^{\mathrm{T}}$ is defined in Table 6.

Due to the far-field shear stress τ^∞, the plate is subjected to mixed-mode deformation involving fracture modes I and II [17]. The mixed-mode stress-intensity factors $K_I(\boldsymbol{X})$ and $K_{II}(\boldsymbol{X})$ were calculated using an interaction integral [18]. The plate was analysed using the finite-element method, involving

Table 5
Failure probability of ten-bar truss structure

Method	Failure probability	Number of function evaluations[a]
MPP-based univariate method with numerical integration		
Linear (Eq. (17))	0.1457	187[b]
Quadratic (Eq. (18))	0.1400	187[b]
MPP-based univariate method with simulation [12]	0.1465	187[b]
FORM	0.0862	127
SORM (Breitung) [4]	0.1286	506
SORM (Hohenbichler) [5]	0.1524	506
SORM (Cai and Elishakoff) [6]	0.1467	506
Direct Monte Carlo simulation	0.1394	1000,000

[a] Total number of times that the original performance function is calculated.
[b] $127 + (n-1) \times N = 127 + (7-1) \times 10 = 187$.

Table 6
Statistical properties of random input for an edge-cracked plate

Random variable	Mean	Standard deviation	Probability distribution
a/W	0.5	0.2309	Uniform[a]
τ^{∞}	Variable[b]	0.1	Gaussian
K_{Ic}	200	0.1	Lognormal

[a] Uniformly distributed over (0.3, 0.7).
[b] Varies from 2.6 to 3.1.

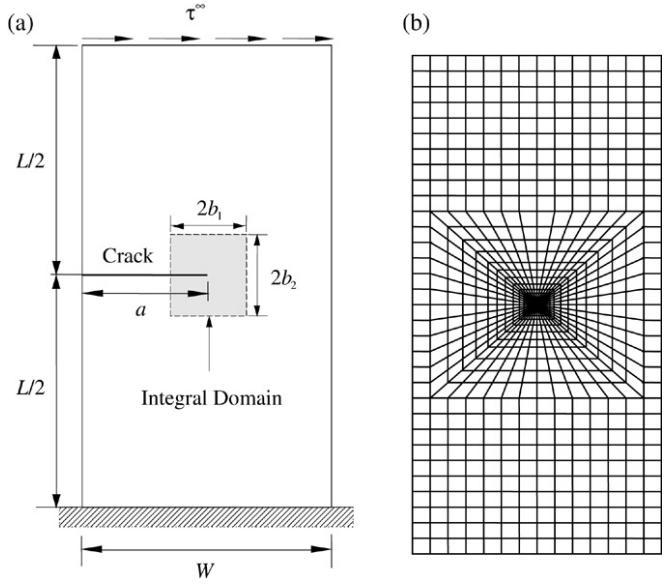

Fig. 5. An edge-cracked plate subject to mixed-mode deformation: (a) geometry and loads; (b) finite-element discretization.

a total of 832 8-noded, regular, quadrilateral elements and 48 6-noded, quarter-point (singular), triangular elements at the crack-tip, as shown in Fig. 5(b).

The failure criterion is based on a mixed-mode fracture initiation using the maximum tangential stress theory [17], which leads to the performance function

$$g(\boldsymbol{X}) = K_{Ic} - \left[K_I(\boldsymbol{X}) \cos^2 \frac{\Theta(\boldsymbol{X})}{2} - \frac{3}{2} K_{II}(\boldsymbol{X}) \sin \Theta(\boldsymbol{X})\right] \cos \frac{\Theta(\boldsymbol{X})}{2}, \quad (24)$$

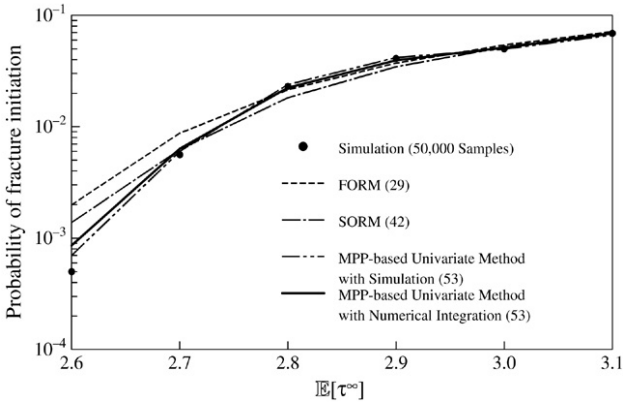

Fig. 6. Probability of fracture initiation in an edge-cracked plate.

where K_{Ic} is the random fracture toughness and $\Theta_c(\boldsymbol{X})$ is the direction of crack propagation.

Failure probability estimates of $P_F = P[g(\boldsymbol{X}) < 0]$, obtained using the proposed univariate method with numerical integration, univariate method using simulation, FORM, Hohenbichler's SORM, and direct Monte Carlo simulation, are compared in Fig. 6 and are plotted as a function of $\mathbb{E}[\tau^{\infty}]$, where $\mathbb{E}$ is the expectation operator. For each reliability analysis (i.e. each point in the plot), FORM and SORM require 29 and 42 function evaluations (finite-element analysis). Using $n = 9$, the MPP-based univariate methods require only 53 (=29 + 24) function evaluations, whereas 50,000 finite-element analyses were employed in the direct Monte Carlo simulation. The results show that both versions of the univariate method are more accurate than other methods, particularly when the failure probability is low. The computational effort by univariate methods is slightly higher than that by FORM/SORM, but much lower than that by direct Monte Carlo simulation.

5.5. Example 5 — Three-span, five-story frame structure

The final example examines the proposed univariate method for solving reliability problems involving correlated random variables. A three-span, five-story frame structure, studied by Liu and Der Kiureghian [19], is subjected to horizontal loads, as shown in Fig. 7. There are 21 random variables: (1) three applied loads, (2) two Young's moduli, (3) eight moments of inertia, and (4) eight cross-sectional areas. The random

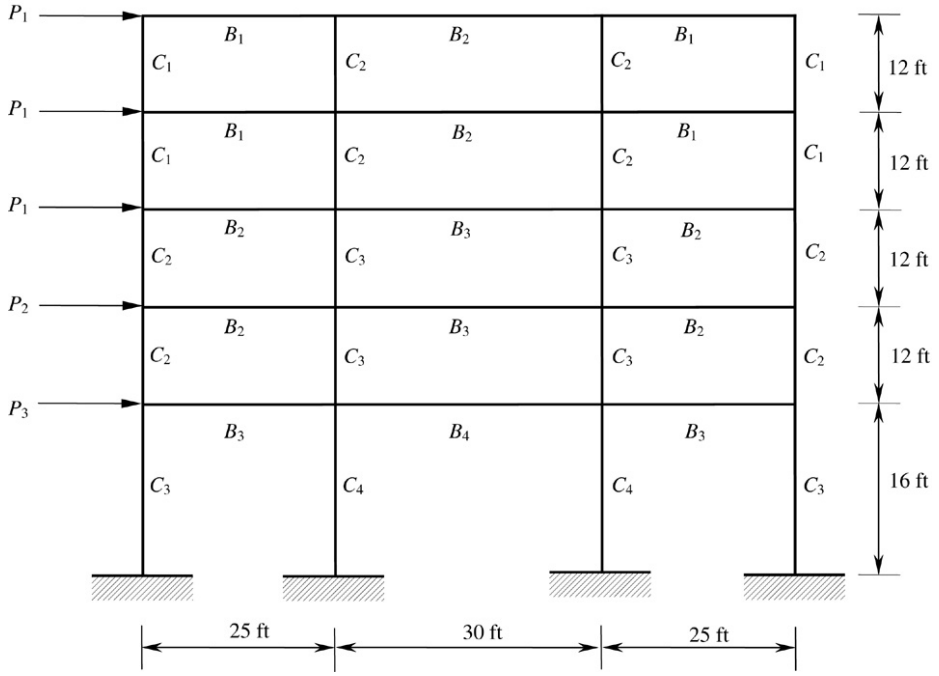

Fig. 7. A three-span, five-story frame structure subjected to lateral loads.

Table 7
Frame element properties

Element	Young's modulus	Moment of inertia	Cross-sectional area
B_1	E_4	I_{10}	A_{18}
B_2	E_4	I_{11}	A_{19}
B_3	E_4	I_{12}	A_{20}
B_4	E_4	I_{13}	A_{21}
C_1	E_5	I_6	A_{14}
C_2	E_5	I_7	A_{15}
C_3	E_5	I_8	A_{16}
C_4	E_5	I_9	A_{17}

variables associated with frame elements are defined in Table 7. Tables 8 and 9 list statistical properties of all random variables. The lognormally distributed load variables are independent and all other random variables are jointly normal. Failure is defined when the horizontal component of the top-floor displacement $u_1(\boldsymbol{X})$ exceeds 0.2 ft, leading to $g(\boldsymbol{X}) = 0.2 - u_1(\boldsymbol{X})$.

The MPP-based univariate methods with numerical integration and simulation, FORM, Hohenbichler's SORM, and direct Monte Carlo simulation were employed to estimate the failure probability and are listed in Table 10. FORM and SORM require 474 and 1143 function evaluations (frame analysis), respectively. Using $n = 7$, the univariate methods require 600 function evaluations, whereas 1,000,000 frame analyses are needed by the direct Monte Carlo simulation. For the univariate method with numerical integration, the linear approximation of $y_N(v_N)$ was employed. The results clearly show that both versions of the univariate method provide more accurate results than FORM and SORM. In terms of effort, the method developed is slightly more expensive than FORM, but significantly more efficient than SORM.

Table 8
Statistical properties of random input for frame structure[a]

Random variable	Mean	Standard deviation	Probability distribution
P_1	30	9	Lognormal
P_2	20	8	Lognormal
P_3	16	6.40	Lognormal
E_4	454,000	40,000	Normal
E_5	497,000	40,000	Normal
I_6	0.94	0.12	Normal
I_7	1.33	0.15	Normal
I_8	2.47	0.30	Normal
I_9	3.00	0.35	Normal
I_{10}	1.25	0.30	Normal
I_{11}	1.63	0.40	Normal
I_{12}	2.69	0.65	Normal
I_{13}	3.00	0.75	Normal
A_{14}	3.36	0.60	Normal
A_{15}	4.00	0.80	Normal
A_{16}	5.44	1.00	Normal
A_{17}	6.00	1.20	Normal
A_{18}	2.72	1.00	Normal
A_{19}	3.13	1.10	Normal
A_{20}	4.01	1.30	Normal
A_{21}	4.50	1.50	Normal

[a] The units of P_i, E_i, I_i, and A_i are kip, kip/ft^2, ft^4, and ft^2, respectively.

In all numerical examples presented, the number of function evaluations required by both versions of the univariate method is the same. However, the present univariate method does not require any Monte Carlo simulations embedded in its previous version. Instead, explicit forms of failure probability requiring only one-dimensional integrations are involved. Hence, the new method should be useful in deriving the sensitivity (gradients) of failure probability for reliability-based design optimization, which is a subject of current research by the authors.

Table 9
Correlation coefficients of random input for frame structure

	P_1	P_2	P_3	E_4	E_5	I_6	I_7	I_8	I_9	I_{10}	I_{11}	I_{12}	I_{13}	A_{14}	A_{15}	A_{16}	A_{17}	A_{18}	A_{19}	A_{20}	A_{21}
P_1	1.0																				
P_2	0.	1.0																			
P_3	0.	0.	1.0																		
E_4	0.	0.	0.	1.0																	
E_5	0.	0.	0.	0.9	1.0																
I_6	0.	0.	0.	0.	0.	1.0															
I_7	0.	0.	0.	0.	0.	0.13	1.0														
I_8	0.	0.	0.	0.	0.	0.13	0.13	1.0													
I_9	0.	0.	0.	0.	0.	0.13	0.13	0.13	1.0												
I_{10}	0.	0.	0.	0.	0.	0.13	0.13	0.13	0.13	1.0											
I_{11}	0.	0.	0.	0.	0.	0.13	0.13	0.13	0.13	0.13	1.0										
I_{12}	0.	0.	0.	0.	0.	0.13	0.13	0.13	0.13	0.13	0.13	1.0									
I_{13}	0.	0.	0.	0.	0.	0.13	0.13	0.13	0.13	0.13	0.13	0.13	1.0								
A_{14}	0.	0.	0.	0.	0.	0.95	0.13	0.13	0.13	0.13	0.13	0.13	0.13	1.0							
A_{15}	0.	0.	0.	0.	0.	0.13	0.95	0.13	0.13	0.13	0.13	0.13	0.13	0.13	1.0						
A_{16}	0.	0.	0.	0.	0.	0.13	0.13	0.95	0.13	0.13	0.13	0.13	0.13	0.13	0.13	1.0					
A_{17}	0.	0.	0.	0.	0.	0.13	0.13	0.13	0.95	0.13	0.13	0.13	0.13	0.13	0.13	0.13	1.0				
A_{18}	0.	0.	0.	0.	0.	0.13	0.13	0.13	0.13	0.95	0.13	0.13	0.13	0.13	0.13	0.13	0.13	1.0			
A_{19}	0.	0.	0.	0.	0.	0.13	0.13	0.13	0.13	0.13	0.95	0.13	0.13	0.13	0.13	0.13	0.13	0.13	1.0		
A_{20}	0.	0.	0.	0.	0.	0.13	0.13	0.13	0.13	0.13	0.13	0.95	0.13	0.13	0.13	0.13	0.13	0.13	0.13	1.0	
A_{21}	0.	0.	0.	0.	0.	0.13	0.13	0.13	0.13	0.13	0.13	0.13	0.95	0.13	0.13	0.13	0.13	0.13	0.13	0.13	1.0

Table 10
Failure probability of frame structure

Method	Failure probability	Number of function evaluations[a]
MPP-based univariate method with numerical integration	3.829×10^{-4}	600[b]
MPP-based univariate method with simulation [12]	3.720×10^{-4}	600[b]
FORM	7.891×10^{-4}	474
SORM (Hohenbichler) [5]	1.402×10^{-4}	1143
Direct Monte Carlo simulation	3.630×10^{-4}	1000,000

[a] Total number of times that the original performance function is calculated.
[b] $474 + (n-1) \times N = 474 + (7-1) \times 21 = 600$.

6. Conclusions

A new univariate method was developed for predicting the component reliability of mechanical systems subject to random loads, material properties, and geometry. The method involves novel function decomposition at the most probable point, which facilitates univariate approximation of a general multivariate function in the rotated Gaussian space and one-dimensional integrations for calculating the failure probability. Based on linear and quadratic approximations of the univariate component function in the direction of the most probable point, two mathematical expressions of the failure probability were derived. In both expressions, the proposed effort in evaluating the failure probability involves calculating conditional responses at a selected input determined by sample points and Gauss–Hermite integration points. The results of five numerical examples involving elementary mathematical functions and structural/solid-mechanics problems indicate that the proposed method provides accurate and computationally efficient estimates of the probability of failure. Compared with the authors' previous work, no Monte Carlo simulation is required in the present version of the univariate method that has been developed. Although both versions of the univariate method have comparable computational efficiencies, the new method should be useful in deriving the sensitivity of the failure probability for reliability-based design optimization, which is the ultimate goal of probabilistic mechanics.

Acknowledgment

The authors would like to acknowledge the financial support of the US National Science Foundation under Grant No. DMI-0355487.

References

[1] Madsen HO, Krenk S, Lind NC. Methods of structural safety. Englewood Cliffs (NJ): Prentice-Hall, Inc.; 1986.
[2] Rackwitz R. Reliability analysis — A review and some perspectives. Structural Safety 2001;23(4):365–95.
[3] Ditlevsen O, Madsen HO. Structural reliability methods. Chichester: John Wiley & Sons Ltd.; 1996.
[4] Breitung K. Asymptotic approximations for multinormal integrals. ASCE Journal of Engineering Mechanics 1984;110(3):357–66.
[5] Hohenbichler M, Gollwitzer S, Kruse W, Rackwitz R. New light on first- and second-order reliability methods. Structural Safety 1987;4:267–84.

[6] Cai GQ, Elishakoff I. Refined second-order reliability analysis. Structural Safety 1994;14:267–76.
[7] Tvedt L. Distribution of quadratic forms in normal space — Application to structural reliability. ASCE Journal of Engineering Mechanics 1990; 116(6):1183–97.
[8] Der Kiureghian A, Dakessian T. Multiple design points in first and second-order reliability. Structural Safety 1998;20(1):37–49.
[9] Nie J, Ellingwood BR. Directional methods for structural reliability analysis. Structural Safety 2000;22:233–49.
[10] Hohenbichler M, Rackwitz R. Improvement of second-order reliability estimates by importance sampling. ASCE Journal of Engineering Mechanics 1988;114(12):2195–8.
[11] Xu H, Rahman S. Decomposition methods for structural reliability analysis. Probabilistic Engineering Mechanics 2005;20:239–50.
[12] Rahman S, Wei D. A univariate approximation at most probable point for higher-order reliability analysis. International Journal of Solids and Structures 2006;43:2820–39.
[13] Xu H, Rahman S. A generalized dimension-reduction method for multi-dimensional integration in stochastic mechanics. International Journal for Numerical Methods in Engineering 2004;61:1992–2019.
[14] Abramowitz M, Stegun I. Handbook of mathematical functions. 9th ed. New York (NY): Dover Publications, Inc.; 1972.
[15] Boresi AP, Schmidt RJ. Advanced mechanics of materials. 6th ed. New York (NY): John Wiley & Sons, Inc.; 2003.
[16] Penmetsa R, Grandhi R. Adaptation of fast Fourier transformations to estimate structural failure probability. Finite Elements in Analysis and Design 2003;39:473–85.
[17] Anderson TL. Fracture mechanics: Fundamentals and applications. 2nd ed. Boca Raton (FL): CRC Press Inc.; 1995.
[18] Yau JF, Wang SS, Corten HT. A mixed-mode crack analysis of isotropic solids using conservation laws of elasticity. Journal of Applied Mechanics 1980;47:335–41.
[19] Liu PL, Der Kiureghian A. Optimization algorithms for structural reliability analysis. Report no. UCB/SESM-86/09. Berkeley (CA); 1986.